Long noncoding RNA *Hoxb3os* is dysregulated in autosomal dominant polycystic kidney disease and regulates mTOR signaling

Received for publication, January 8, 2018, and in revised form, April 19, 2018 Published, Papers in Press, May 1, 2018, DOI 10.1074/jbc.RA118.001723

Karam Aboudehen[‡1], Shayan Farahani[‡], Mohammed Kanchwala[§], Siu Chiu Chan[‡], Svetlana Avdulov[‡], Alan Mickelson[‡], Dayeon Lee[‡], Micah D. Gearhart[¶], Vishal Patel[‖], Chao Xing[§‡‡], and Peter Igarashi[‡]**

*From the [‡]Department of Medicine and [¶]Department of Genetics, Cell Biology, and Development, University of Minnesota, Minneapolis, Minnesota, 55455 and [§]McDermott Center for Human Growth and Development and Departments of [‡‡]Clinical Sciences, **Bioinformatics, and [‖]Internal Medicine, UT Southwestern Medical Center, Dallas, Texas 75390*

Edited by Karin Musier-Forsyth

Autosomal dominant polycystic kidney disease (ADPKD) is a debilitating disease that is characterized by the accumulation of numerous fluid-filled cysts in the kidney. ADPKD is primarily caused by mutations in two genes, *PKD1* and *PKD2*. Long noncoding RNAs (lncRNA), defined by a length >200 nucleotides and absence of a long ORF, have recently emerged as epigenetic regulators of development and disease; however, their involvement in PKD has not been explored previously. Here, we performed deep RNA-Seq to identify lncRNAs that are dysregulated in two orthologous mouse models of ADPKD (kidney-specific *Pkd1* and *Pkd2* mutant mice). We identified a kidney-specific, evolutionarily conserved lncRNA called *Hoxb3os* that was down-regulated in cystic kidneys from *Pkd1* and *Pkd2* mutant mice. The human ortholog *HOXB3-AS1* was down-regulated in cystic kidneys from ADPKD patients. *Hoxb3os* was highly expressed in renal tubules in adult WT mice, whereas its expression was lost in the cyst epithelium of mutant mice. To investigate the function of *Hoxb3os*, we utilized CRISPR/Cas9 to knock out its expression in mIMCD3 cells. Deletion of *Hoxb3os* resulted in increased phosphorylation of mTOR and its downstream targets, including p70 S6 kinase, ribosomal protein S6, and the translation repressor 4E-BP1. Consistent with activation of mTORC1 signaling, *Hoxb3os* mutant cells displayed increased mitochondrial respiration. The *Hoxb3os* mutant phenotype was partially rescued upon re-expression of *Hoxb3os* in knockout cells. These findings identify *Hoxb3os* as a novel lncRNA that is down-regulated in ADPKD and regulates mTOR signaling and mitochondrial respiration.

Autosomal dominant polycystic kidney disease (ADPKD)[2] is one of the most common monogenic diseases, affecting 1 in 800–1000 people worldwide, and is the fourth-leading cause of end-stage renal failure (1, 2). ADPKD is caused primarily by mutations in *PKD1* or *PKD2* (3). The typical renal phenotype of ADPKD is the insidious development of hundreds of renal cysts. Cysts begin forming during early stages of development and grow progressively throughout the life of the individual (4, 5). About half of those affected with ADPKD will progress to end-stage renal failure necessitating dialysis or kidney transplantation (6).

The functions of the PKD1 and PKD2 gene products are incompletely understood. *PKD1* encodes polycystin-1, a large glycoprotein with an N-terminal extracellular region containing protein-protein interaction motifs, a transmembrane domain, and a C-terminal cytoplasmic tail (7, 8). *PKD2* encodes polycystin-2, a Ca^{2+}-permeable cation channel that interacts with, and is regulated by, polycystin-1 (9–11). A common consequence of malfunction of the polycystin-1/2 complex is reduced intracellular Ca^{2+} levels and increased levels of cAMP (12, 13). PKD1 and PKD2 regulate multiple signaling pathways that maintain normal tubular structure and function (14). For example, some mutant mice display defects in growth factor/receptor tyrosine kinase pathways (15), whereas others have abnormalities in Wnt/β-catenin signaling (16), and in the mTOR pathway (17). It is still unclear which pathways are primarily involved in pathogenesis and which ones are affected secondarily.

Long noncoding RNAs (lncRNAs) are a class of nonprotein-coding RNAs that are >200 nucleotides in length and are characterized by the absence of a long ORF (18). LncRNAs function as activators, guides, or scaffolds for transcription factors and histone modifiers. They also play important roles in posttranscriptional regulation by affecting mRNA activity and stability, as well as translational efficiency (19). LncRNAs have been implicated in a range of diseases, including cancer (20). However, their involvement in ADPKD has not been reported previously. LncRNAs are attractive therapeutic targets because

This work was supported by the National Institutes of Health Grants R37DK042921 (to P. I.) and UL1TR001105 (to C. X.). The authors declare that they have no conflicts of interest with the contents of this article. The content is solely the responsibility of the authors and does not necessarily represent the official views of the National Institutes of Health.

The RNA sequences for this project can be accessed through the NCBI under Gene Expression Omnibus accession number GSE108864.

This article contains Figs. S1–S6.

[1] To whom correspondence should be addressed: 420 Delaware St. SE, MMC 605, Minneapolis, MN. Tel.: 612-625-0530; E-mail: karam@umn.edu.

[2] The abbreviations used are: ADPKD, autosomal dominant polycystic kidney disease; lncRNAs, long noncoding RNAs; PhyloCSF, phylogenetic codon substitution frequency software; qRT-PCR, quantitative RT-PCR; RACE, rapid amplification of cDNA ends; P, postnatal; E, embryonic; ISH, *in situ* hybridization; ECAR, extracellular acidification rate; OCR, oxygen consumption rates; p-, phospho-; FCCP, carbonyl cyanide p-trifluoromethoxyphenylhydrazone; ROS, reactive oxygen species; sgRNAs, single guide RNAs.

they can regulate multiple genes and pathways that are affected in a disease, and their activity can be modulated *in vivo* (21–23). Recent studies reveal that lncRNAs are dysregulated in human diseases. For example, lnc-PCA3 promotes aggressive prostate cancer and is up-regulated 60-fold in prostate tumors compared with normal tissue (24). Another lncRNA, *MALAT1*, is overexpressed in lung cancer (25), bladder cancer (26), liver cancer (27), and colorectal cancer (28). *MALAT1* is regarded as a decisive regulator of metastasis in lung cancer cells (29). Recent evidence suggests that lncRNAs play a significant role in kidney diseases. For example, *Tug1* is an lncRNA that improves diabetic nephropathy in the mouse kidney by regulating mitochondrial bioenergetics (30). These findings make lncRNAs attractive targets for efforts aimed at improving ADPKD treatment.

In this study, we have identified a kidney-specific, evolutionarily conserved lncRNA called *Hoxb3os*, which is down-regulated in two orthologous mouse models of ADPKD (kidney-specific *Pkd1* and *Pkd2* mutant mice). Knockout of *Hoxb3os* with CRISPR/Cas9 in mIMCD3 kidney epithelial cells results in hyperactivation of mTOR signaling, and increased rates of oxygen consumption. Conversely, re-expression of *Hoxb3os* in knockout cells partially rescues the mutant phenotype. These findings identify *Hoxb3os* as an lncRNA that is down-regulated in ADPKD and negatively regulates mTOR signaling.

Results

Identification of lncRNAs that are dysregulated in Pkd1 and Pkd2 mutant kidneys

Our laboratory has previously generated two mouse models of ADPKD: Ksp/Cre;*Pkd1*$^{f/f}$ mice (*Pkd1*-KO), in which *Pkd1* is deleted in renal tubules, and Pkhd1/Cre;*Pkd2*$^{f/f}$ mice (*Pkd2*-KO), in which *Pkd2* is deleted in collecting ducts (31, 32). Compared with WT mice, extensive renal cyst formation was present in *Pkd1*-KO kidney at postnatal day 10 (P10) and in *Pkd2*-KO kidney at P21 (Fig. 1*A*). To identify lncRNAs that are dysregulated in both KO mouse models, we conducted whole-transcriptome analysis (RNA-Seq) of RNA from WT, *Pkd1*-KO, and *Pkd2*-KO kidneys. We discovered 120 lncRNAs that were dysregulated in *Pkd1*-KO kidneys and 135 that were dysregulated in *Pkd2*-KO kidneys ($p < 0.05$, log cpm > -1). Sixty-six lncRNAs were similarly dysregulated in both models, and 41 showed >2-fold change in expression (Fig. 1*B*). Next, we sought to identify novel lncRNAs that are dysregulated in ADPKD by performing *de novo* transcriptome assembly. We identified 358 previously unannotated transcripts from mouse adult kidney. These putative transcripts were then filtered to distinguish transcripts that might encode proteins from those that are non-coding. We used the phylogenetic codon substitution frequency software (PhyloCSF) (33) to assess the protein-coding potential of each transcript. Twenty-four transcripts had protein-coding potential and were excluded from further analysis. Of the remaining transcripts, 139 were dysregulated in *Pkd1*-KO kidneys and 106 were dysregulated in *Pkd2*-KO kidneys ($p < 0.05$, log cpm > -1). Sixty unique transcripts were dysregulated in both animal models, and 50 displayed more than 2-fold change in expression (Fig. 1*C*). The majority of the

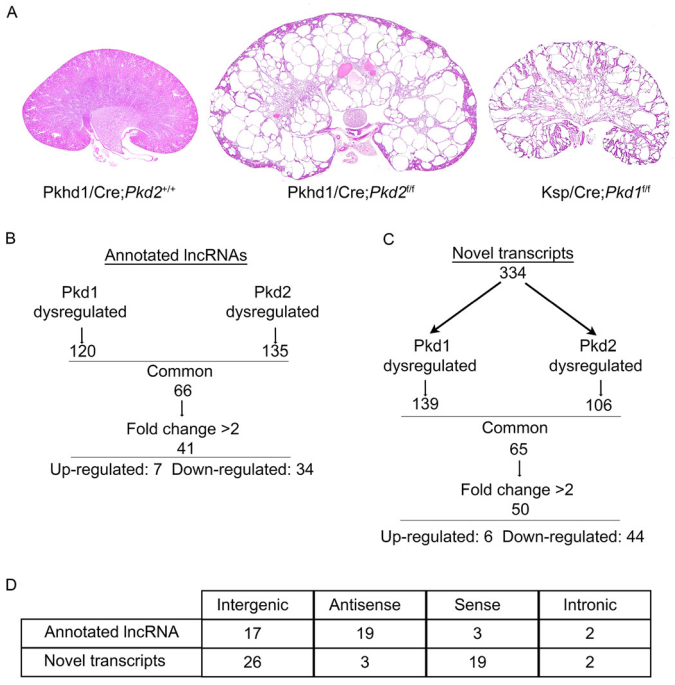

D

	Intergenic	Antisense	Sense	Intronic
Annotated lncRNA	17	19	3	2
Novel transcripts	26	3	19	2

Figure 1. Identification of lncRNAs that are dysregulated in mouse models of ADPKD. *A*, kidney-specific inactivation of *Pkd1* (Ksp/Cre;*Pkd1*$^{f/f}$) at postnatal day 10 (P10) and *Pkd2* (Pkhd1/Cre;*Pkd2*$^{f/f}$) at P20 produces kidney cysts compared with control (Pkhd1/Cre;*Pkd2*$^{+/+}$). Kidneys were stained with H&E. *B* and *C*, identification by pair-end RNA-Seq of annotated (*B*) and novel (*C*) lncRNAs that are dysregulated in both *Pkd1* and *Pkd2* mutant kidneys ($p < 0.05$, log cpm > -1). *D*, mapping of dysregulated lncRNAs to genomic regions relative to protein-coding genes.

novel transcripts were down-regulated, whereas six were up-regulated. Mapping of the lncRNAs to the mouse genome revealed that most annotated lncRNAs were classified as antisense and intergenic, whereas the majority of the novel transcripts were classified as sense and intergenic (Fig. 1*D*).

Characterization of lncRNAs in the mouse kidney

We characterized the expression of the 41 known lncRNAs that were highly dysregulated in both *Pkd1*-KO and *Pkd2*-KO kidneys. We first determined the developmental pattern of expression by performing quantitative RT-PCR (qRT-PCR) on RNA from embryonic (E16.5), newborn (P1), and adult (P30) mouse kidney. Our results show that the majority of lncRNAs in the mouse kidney were developmentally regulated. Twenty-seven lncRNAs were up-regulated, 10 were down-regulated, and 4 were unchanged between E16.5 and P30 (Fig. S1). Next, we compared expression of the dysregulated lncRNAs in the kidney relative to five other organs in the mouse. The majority of lncRNAs were expressed in all six organs, whereas five were kidney-specific (Fig. S2). We then examined the subcellular localization of lncRNAs by performing RNA fractionation in WT adult mouse kidney tissue. Fractionation experiments revealed that 32 lncRNAs were predominantly nuclear and 9 were predominantly cytoplasmic (Fig. S3).

Identification of Hoxb3os as a candidate lncRNA in the pathogenesis of ADPKD

Hoxb3os was among the most dysregulated lncRNAs that were identified in our screen. *Hoxb3os* is an antisense transcript

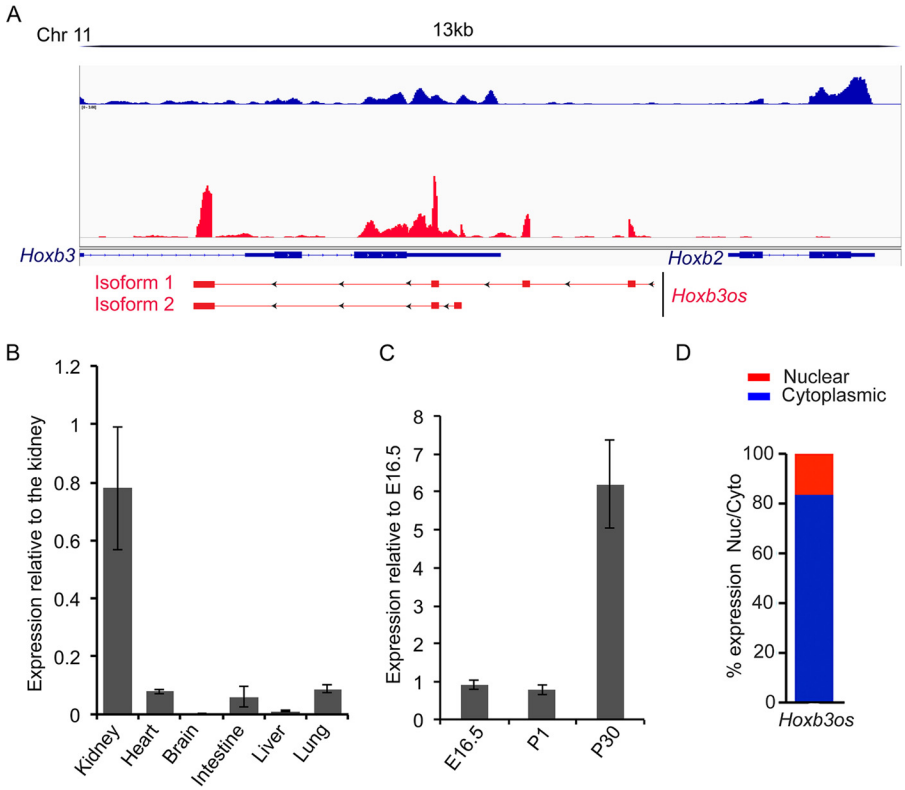

Figure 2. Expression of *Hoxb3os* in the mouse kidney. *A*, RACE identifies two major *Hoxb3os* isoforms in the mouse kidney. *Upper panel* shows RNA-Seq reads from a WT kidney visualized with Integrative Genomics Viewer software (*blue bars* indicate reads from positive strand and *red bars* indicate negative strand). The two *Hoxb3os* isoforms (*lower panel*) are located 5′ to *Hoxb2* and partially overlap with *Hoxb3* (*arrowheads* indicate direction of transcription and *solid rectangles* indicate exons). *B*, quantitative RT-PCR showing expression of *Hoxb3os* in different mouse organs relative to the kidney. *C*, developmental expression of *Hoxb3os* in the embryonic (E16.5), newborn (P1), and adult (P30) mouse kidney measured by qRT-PCR. *D*, percentage of *Hoxb3os* expression in cytoplasmic and nuclear fractions from an adult mouse kidney measured by qRT-PCR. *Error bars* indicate S.E.

that is located on chromosome 11 and spans a genomic region of about 7 kb. *Hoxb3os* is located 5′ to *Hoxb2* and partially overlaps with the 3′-end of *Hoxb3* (Fig. 2*A*). Rapid amplification of cDNA ends (RACE) in the adult mouse kidney showed that *Hoxb3os* exists as two major isoforms that are transcribed from two distinct promoter regions. *Hoxb3os* isoform 1, which constitutes the longest transcript (557 nucleotides), comprises four exons and represents the major fraction of the total transcript as determined by qRT-PCR. Expression analysis revealed that *Hoxb3os* was highly abundant in the normal kidney but was almost undetectable in five other organs (Fig. 2*B*). In addition, expression of *Hoxb3os* was developmentally up-regulated between E16.5 and adult kidney (Fig. 2*C*). In contrast, the nearby protein-coding genes, *Hoxb2* and *Hoxb3*, were developmentally down-regulated (Fig. S4*A*). RNA fractionation experiment revealed that 80% of spliced *Hoxb3os* transcripts were localized to the cytoplasm and 20% were nuclear (Fig. 2*D*).

Hoxb3os is down-regulated in cystic kidney

RNA-Seq studies revealed that *Hoxb3os* was down-regulated in both *Pkd1*-KO and *Pkd2*-KO kidneys. We performed qRT-PCR and confirmed down-regulation of *Hoxb3os* by 90% in *Pkd1*-KO kidneys and by 75% in *Pkd2*-KO kidneys (Fig. 3*A*). We also measured *Hoxb3os* expression before the onset of cyst formation in *Pkd2*-KO kidney at P10. Relative to WT kidney, expression of *Hoxb3os* was reduced by 35% in the pre-cystic kidney (Fig. 3*B*). *Hoxb3os* was also down-regulated in a *Pkd2*-null kidney cell line (Fig. 3*C*). We determined the localization of *Hoxb3os* in the normal and cystic kidney by *in situ* hybridization (ISH) utilizing a probe that recognizes both *Hoxb3os* isoforms. ISH revealed that *Hoxb3os* was expressed in epithelial tubules of the normal kidney (Fig. 3, *D* and *E*). In cystic kidneys, expression of *Hoxb3os* was significantly reduced throughout the kidney and was almost undetectable within the epithelial lining of the cysts (Fig. 3, *F* and *G*). In contrast to the decreased expression of *Hoxb3os* in *Pkd1* and *Pkd2* mutant kidneys, the expression of *Hoxb2* was up-regulated and *Hoxb3* was unchanged (Fig. S4*C*).

Because *Hoxb3os* is highly evolutionarily conserved, we measured the expression of its human ortholog, *HOXB-AS1* (34), in human *ADPKD*. *HOXB-AS1* comprises four transcripts that partially overlap with *HOXB2* and *HOXB3* (Fig. S5*A*). Expression analysis utilizing primer sets that detected multiple *HOXB-AS1* isoforms revealed that *HOXB-AS1* was down-regulated by 60% in cystic kidneys from humans with ADPKD (Fig. S5*B*). Similar to results in the mouse, the expression of the protein-coding gene *HOXB2* was up-regulated and the expression of *HOXB3* was unchanged in cystic human kidneys (Fig. S4*D*).

Hoxb3os regulates a network of genes and signaling pathways that are commonly altered in ADPKD

To determine the function of *Hoxb3os*, we inhibited its expression in mIMCD3 renal epithelial cells using GapmeRs, which are potent antisense oligonucleotides (Exiqon). Trans-

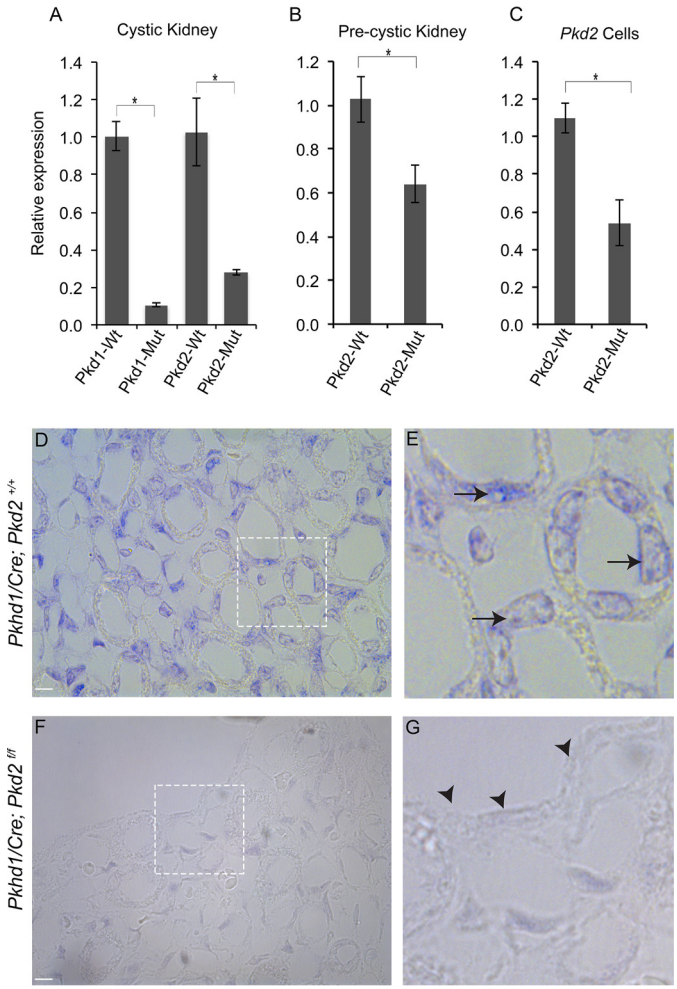

Figure 3. Down-regulation of *Hoxb3os* in cystic kidney. *A–C*, quantitative RT-PCR showing decreased expression of *Hoxb3os* in cystic kidneys from *Pkd1* (P10) and *Pkd2* (P20) mutant mice (*A*), pre-cystic *Pkd2* mutant kidney at P10 (*B*), and *Pkd2* mutant cells (*C*). *D–G*, *in situ* hybridization showing down-regulation of *Hoxb3os* in cystic kidneys (Pkhd1/Cre;*Pkd2*$^{f/f}$) (*F* and *G*) compared with control kidneys (Pkhd1/Cre;*Pkd2*$^{+/+}$) (*D* and *E*) at P15. *Insets* show higher magnification images. *Arrows* show expression in kidney tubules, and *arrowheads* indicate loss of expression within the epithelial lining of the cyst. *Scale bar* is 5 μm. *Error bars* indicate S.E. *, $p < 0.05$.

fection with GapmeRs against *Hoxb3os* reduced levels of the mature transcript by 65% (Fig. 4*A*). Next, we performed RNA-Seq to identify genes that are differentially expressed in response to *Hoxb3os* knockdown. A total of 1964 genes were differentially expressed between knockdown and control cells (false discovery rate <0.05). The expression of 77 genes changed by more than 2-fold between control and knockdown cells (Fig. 4*B*). Importantly, expression of 40 of these genes was also altered *in vivo* in cystic kidneys from *Pkd1*-KO and *Pkd2*-KO mice (Fig. 4*C*). We then performed pathway analysis on the complete set of genes that were differentially expressed in knockdown cells ($n = 1964$). This analysis identified EIF2, mTOR, EIF4, and P70S6K signaling as the most dysregulated pathways in *Hoxb3os* mutant cells (Fig. 4*D*). These pathways are involved in enhanced anabolic processes such as mRNA translation, and share a common gene-signature profile. To determine whether the predicted dysregulations in pathways translated to molecular alterations, we measured the levels of mTOR and phosphorylated mTOR (p-mTOR). Western blot analysis revealed that p-mTOR was increased in cell lysates from *Hoxb3os* knockdown (Fig. 4*E*). These data suggested that *Hoxb3os* regulates mTOR signaling.

Ablation of Hoxb3os results in hyperactivation of mTORC1 and enhanced mitochondrial respiration

To confirm that *Hoxb3os* regulates mTOR signaling, we used CRISPR/Cas9 gene editing to ablate *Hoxb3os* in mIMCD3 cells. We designed single guide RNAs (sgRNAs) to remove the endogenous promoter and first exon of isoform 1 of *Hoxb3os* (Fig. S6*A*). Because expression of *Hoxb3os* isoform 2 was not detected in mIMCD3 cells (data not shown), only isoform 1 was targeted. Successful deletion of the *Hoxb3os* locus (*Hoxb3os*-KO) was confirmed by PCR analysis on genomic DNA (Fig. S6*B*). To determine the effect of genomic deletion on the *Hoxb3os* transcript, we performed qRT-PCR using primer sets designed to amplify different exons. Elimination of the full-length *Hoxb3os* transcript that harbors the first exon was confirmed by qPCR. However, low levels of a truncated transcript that harbors downstream exons were detected, indicating that expression was not completely abolished (Fig. S6*C*). Quantitative RT-PCR showed that similar to *Hoxb3os*-KD cells, the expression of genes in the mTOR pathway was dysregulated in *Hoxb3os*-KO cells (Fig. S6*E*). Importantly, the expression of nearby protein-coding genes, *Hoxb2* and *Hoxb3*, was unaltered in *Hoxb3os*-KO cells (Fig. S4*B*), which indicates that *Hoxb3os* is unlikely to regulate the transcription of *Hoxb2* and *Hoxb3*.

mTOR exists in two distinct multiprotein complexes (mTORC1 and mTORC2) (35). Phosphorylation of p70S6 kinase (p-S6K), ribosomal S6 protein (p-RS6), and eukaryotic translation initiation factor 4E–binding protein 1 (p-4E–BP1) are known downstream targets of mTORC1 (36), whereas phosphorylation of AKT at Ser-473 is targeted by mTORC2 (37). Western blot analysis of lysates from *Hoxb3os*-KO and WT cells revealed that ablation of *Hoxb3os* increased the levels of p-mTOR, p-S6K, p-RS6, and p-4E–BP1 at Ser-65 (Fig. 5*A*). The levels of the nonphosphorylated forms of these proteins did not change nor did the phosphorylation of AKT at Ser-473 (data not shown). These results suggest that *Hoxb3os* regulates the activity of mTORC1 but not mTORC2. A key physiological readout of mTORC1 activation is enhanced cell metabolism (38). To uncover metabolic differences between WT and *Hoxb3os*-KO cells, we measured extracellular acidification (ECAR) and oxygen consumption (OCR) rates. Compared with WT cells, *Hoxb3os*-KO cells displayed increased mitochondrial respiration as evidenced by higher OCR at baseline and upon addition of FCCP, an uncoupling agent that increases proton permeability and dissociates the electron transport chain from ATP production (Fig. 5*B*). The enhanced cellular respiration is consistent with activation of mTORC1 signaling in *Hoxb3os*-KO cells. *Hoxb3os*-KD cells also showed increased OCR, although the change was not statistically significant, presumably because of incomplete inhibition in KD cells (data not shown).

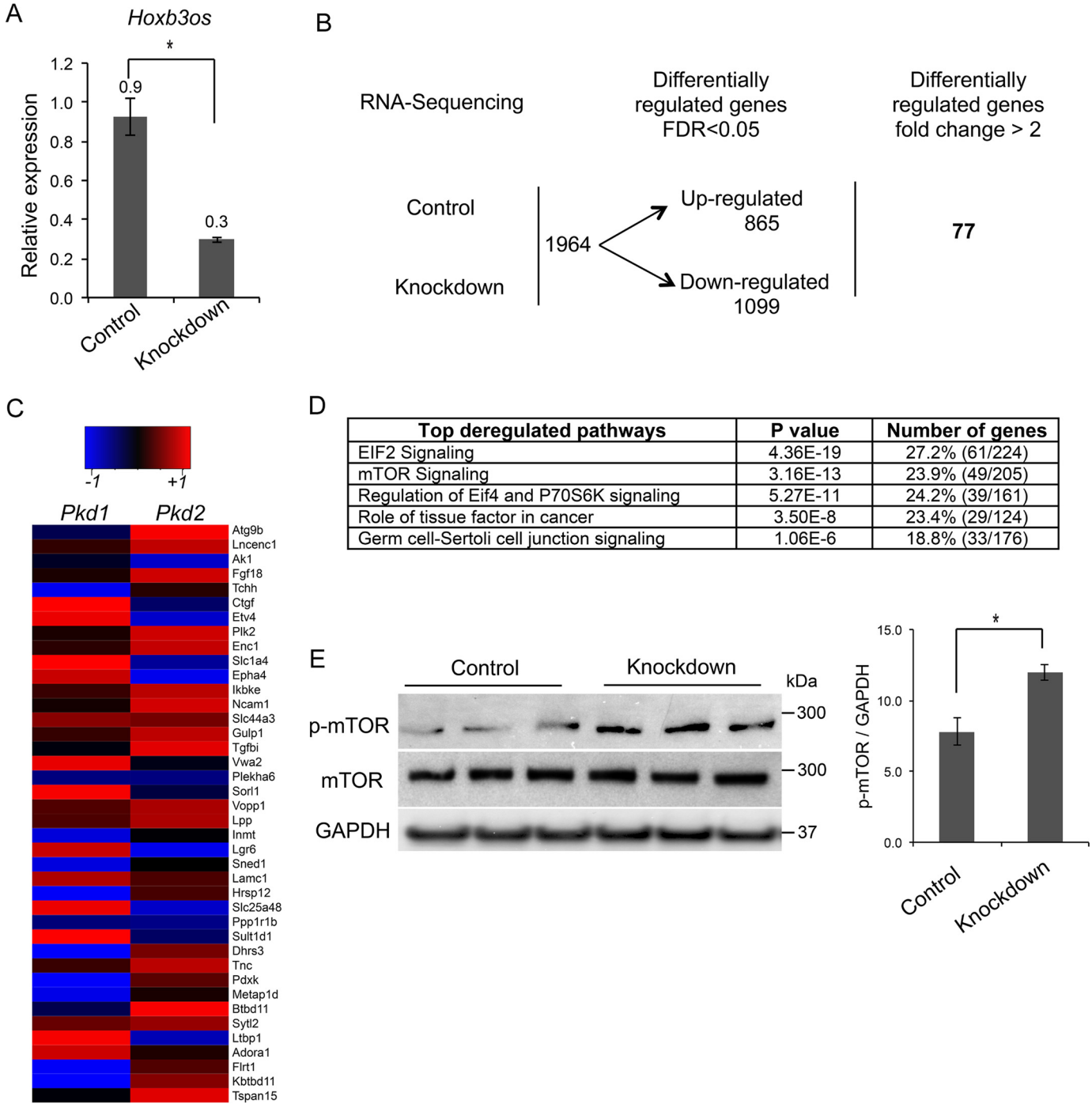

Top deregulated pathways	P value	Number of genes
EIF2 Signaling	4.36E-19	27.2% (61/224)
mTOR Signaling	3.16E-13	23.9% (49/205)
Regulation of Eif4 and P70S6K signaling	5.27E-11	24.2% (39/161)
Role of tissue factor in cancer	3.50E-8	23.4% (29/124)
Germ cell-Sertoli cell junction signaling	1.06E-6	18.8% (33/176)

Figure 4. Knockdown of *Hoxb3os* in kidney cells results in abnormal mTOR signaling. *A*, treatment of mIMCD3 cells with GapmeRs decreases *Hoxb3os* expression levels by more than 60% as measured by qRT-PCR. *B*, RNA-Seq reveals differential expression of genes between *Hoxb3os* knockdown and control mIMCD3 cells ($n = 3$). *C*, heat map showing most deregulated genes in response to *Hoxb3os* knockdown that were also altered in both *Pkd1* and *Pkd2* cystic kidneys ($n = 40$). *D*, pathway analysis using Ingenuity Pathway Analysis (IPA) of differentially regulated genes indicating the most affected signaling pathways in *Hoxb3os* knockdown cells. *E*, Western blot analysis demonstrates an increase in the phosphorylation of mTOR (p-mTOR) in response to knockdown of *Hoxb3os*. *Right panel* shows densitometric analysis of the Western blots. *Error bars* indicate S.E. *, $p < 0.05$.

Re-expression of Hoxb3os in knockout cells partially rescues mTOR signaling and mitochondrial respiration

Next, we tested whether restoring the expression of *Hoxb3os* in knockout cells rescues the abnormalities in mTOR signaling and mitochondrial respiration. We cloned full-length *Hoxb3os* into a lentiviral vector containing a modified backbone that is suitable for lncRNA expression (39). The resulting vector (LeGO-*Hoxb3os*) featured a spleen focus-forming virus promoter (SFFV) that drives the expression of *Hoxb3os* at levels similar to its endogenous expression. In addition, the LeGO-*Hoxb3os* vector included a poly(A) signal immediately downstream of the *Hoxb3os* insert that prevented transcription of adjacent proviral DNA and maintained the secondary structure of *Hoxb3os*. We established three independent cell lines with

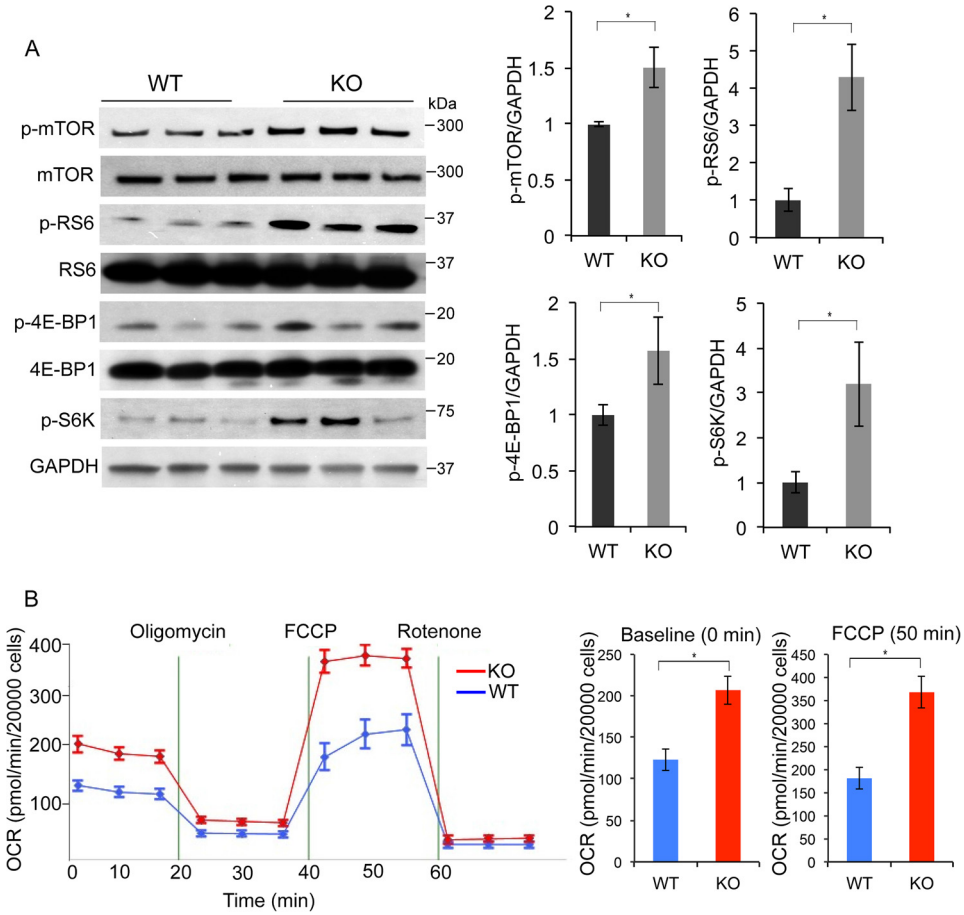

Figure 5. Ablation of *Hoxb3os* in kidney cells results in up-regulation of mTOR signaling and enhanced mitochondrial respiration. *A*, Western blot analysis showing the levels of mTOR and p-mTOR, RS6, and p-RS6, eukaryotic translation initiation factor 4E-BP1 and p-4E-BP1, p-S6K, and GAPDH in WT and *Hoxb3os* knockout (*KO*) cells. *Right panel* shows densitometric analysis of the Western blots. *B*, measurement of OCR in WT (*blue*) and *Hoxb3os* KO (*red*) cells under basal conditions and in response to the indicated mitochondrial inhibitors. Addition of the protonophore FCCP reveals the maximal respiratory capacity of the cells. The rate of respiration at baseline and in response to FCCP is quantified in the *right panel*. *Error bars* indicate S.E. *, $p < 0.05$.

stable expression of *Hoxb3os*. qRT-PCR confirmed re-expression of *Hoxb3os* transcript in the original *Hoxb3os*-KO cells at a level similar to WT mIMCD3 cells (Fig. S4*D*). To determine whether restoring *Hoxb3os* expression in *Hoxb3os*-KO cells rescued the increase in mTOR signaling, we performed Western blot analysis on lysates from *Hoxb3os*-KO cells transduced with either LeGO-*Hoxb3os* (*Hoxb3os*-rescued) or LeGO-empty (nonrescued) vector. Compared with nonrescued cells, *Hoxb3os*-rescued cells displayed lower levels of p-mTOR, p-S6K, and p-RS6. No difference was observed in p-4E–BP1 at Ser-65 levels (Fig. 6*A*). Next, we measured ECAR and OCR in nonrescued and *Hoxb3os*-rescued cells. Compared with nonrescued cells, *Hoxb3os*-rescued cells displayed significantly lower OCR levels, both at baseline and after FCCP treatment (Fig. 6*B*). Furthermore, OCR levels in rescued cells were similar to WT cells at baseline, but remained higher after addition of FCCP (Fig. 6*B*). These data further confirm that *Hoxb3os* is a negative regulator of mTORC1 signaling and mitochondrial respiration.

Discussion

In this study, we comprehensively identified lncRNAs that are dysregulated in mouse models of ADPKD. Utilizing two independent and orthologous mouse models is a powerful approach to discover lncRNAs that are implicated in the pathogenesis of ADPKD. A total of 120 and 135 lncRNA were dysregulated in *Pkd1*-KO and *Pkd2*-KO mice, respectively. Among the differentially expressed lncRNAs, 77 were commonly dysregulated, and 41 displayed more than 2-fold change in expression. Endogenous lncRNAs are expressed at low levels, and studies suggest that the contribution of lncRNAs in a disease process is modest in many cases. Our aim was to discover lncRNAs that could potentially be pathogenic in ADPKD; as a result, we focused on identifying targets that are highly expressed and significantly dysregulated in ADPKD. The stringency of our selection criteria was reflected by the relatively small number of annotated transcripts that were identified in our screen.

We specifically focused on investigating *Hoxb3os,* a lncRNA of unknown function, which is highly down-regulated in both *Pkd1*-KO and *Pkd2*-KO kidneys. *Hoxb3os* was a compelling lncRNA in our study for the following reasons: 1) evolutionarily conserved and abundantly expressed within the kidney epithelium, 2) dysregulated in both cystic and pre-cystic kidneys, 3) loss of expression in the cyst lining, and 4) decreased expression

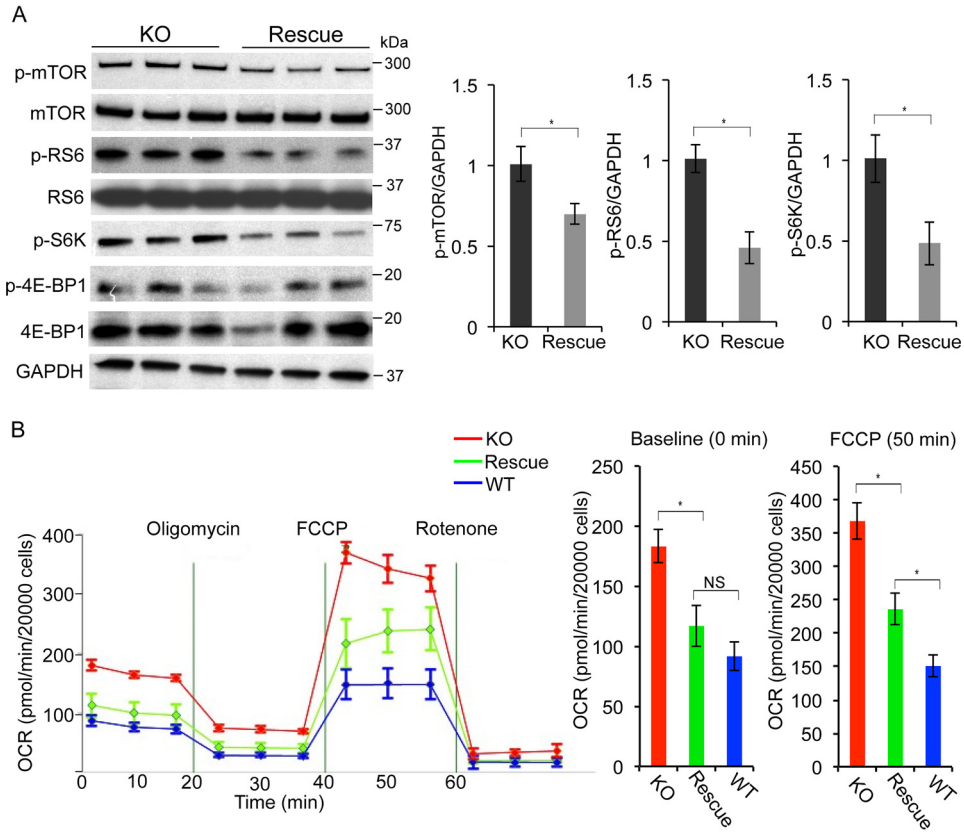

Figure 6. Re-expression of *Hoxb3os* in knockout cells partially rescues mTOR signaling and mitochondrial respiration. *A*, Western blot analysis showing lower levels of p-mTOR, p-RS6, and p-S6K in knockout cells transfected with *Hoxb3os*-expressing lentiviral construct (*Rescue*) compared with cells transfected with the empty lentiviral construct (*KO*). *Right panel* shows densitometric analysis of the Western blots. *B*, measurement of OCR in nonrescued (*red*), rescued (*green*), and WT (*blue*) cells demonstrate partial restoration of OCR to WT levels in rescued compared with nonrescued cells. The rate of respiration at baseline and in response to FCCP is quantified in the *right panel*. *Error bars* indicate S.E. *, $p < 0.05$. *NS*, not significant.

of its human ortholog, *HOXB-AS1,* in kidneys from ADPKD patients. We uncovered a novel role for *Hoxb3os* in regulating mTOR pathway and metabolism in mouse kidney cells. Our results reveal that *Hoxb3os* is a negative regulator of mTORC1 activity and mitochondrial respiration. The evidence for our findings is demonstrated using two experimental approaches: 1) knockdown and genetic deletion of *Hoxb3os* in kidney cells resulted in enhanced mTORC1 activity and mitochondrial respiration, and 2) re-expression of *Hoxb3os* transcript in the knockout cells using lentiviral vector partially rescued the *Hoxb3os*-mutant phenotype.

Hoxb3os is located on chromosome 11 within the *HoxB* cluster of homeotic genes. Recent studies reveal that lncRNAs embedded within the *HOX* cluster of homeotic genes possess critical gene-regulatory functions through both cis and trans mechanisms on *HOX* and non-*HOX* genes. For example, *Hotair* is located in the *HoxC* cluster and is expressed in distal limb buds and posterior trunk of the developing mouse. Deletion of *Hotair* in the mouse resulted in vertebral transformations and abnormal development of metacarpals and carpals (40). A similar mutant phenotype was reported for the *HoxA*-associated lncRNA *Hottip* (41). In our study, knockout of *Hoxb3os* in kidney cells did not affect the expression of the overlapping *Hoxb3* gene. Expression of *Hoxb3* was developmentally regulated, but its expression was unchanged in *Pkd1* and *Pkd2* mutant kidneys. These results suggest that dysregulation of *Hoxb3* is unlikely to explain the pathological effects of *Hoxb3os* dysregulation. However, 77 genes displayed more than 2-fold change in expression in response to *Hoxb3os* knockdown. These results suggest that *Hoxb3os* may exert transcriptional effects in trans toward distant promoters. Moreover, 40 genes that represented more than 50% of the highly dysregulated targets ($n = 77$) were also changed in both *Pkd1* and *Pkd2* mutant kidneys. These findings indicate a similarity in the transcriptional alterations between *Hoxb3os* knockdown cells and ADPKD and suggest that a subset of the dysregulated genes in *Pkd1* and *Pkd2* mutant kidneys may result from altered *Hoxb3os* expression.

Pathway analysis of RNA-Seq data from *Hoxb3os* knockdown cells identified defects in signaling networks that are involved in translational control, including the mTOR pathway. The predicted changes in mTOR signaling translated into alteration at the molecular level, whereby phospho-mTOR levels were significantly induced in response to *Hoxb3os* knockdown. We used CRISPR/Cas9 gene editing to delete *Hoxb3os* in mIMCD3 cells and confirmed regulation of the mTOR pathway. Similar to knockdown cells, ablation of the first exon and promoter region of *Hoxb3os* isoform 1 resulted in increased p-mTOR levels. We next focused on mapping additional proteomic and phosphoproteomic changes within the mTOR pathway as a result of *Hoxb3os* deficiency. We found an increase in phosphorylation of downstream effectors of

mTORC1, including p-S6K, p-RS6, and p-4E–BP1. No changes were observed in proteins that are upstream regulators of mTOR (ERK1/2 and RHEB) as well as those that are known to function in mTORC2 (IRS2 and p-AKT at Ser-473) (data not shown). Taken together, our data suggest that *Hoxb3os* specifically regulates the activity of mTORC1 but not mTORC2. mTOR hyperactivation has been reported in many mouse models of ADPKD, including *Pkd1*-KO and *Pkd2*-KO mouse models (42). Although clinical trials with mTOR inhibitors have produced mixed results, a recent study showed that low-dose rapamycin (mTOR inhibitor) improved kidney function (43). We are currently investigating whether down-regulation of *Hoxb3os* contributes to mTOR hyperactivation and cyst progression in ADPKD. Other studies have reported regulation of mTOR signaling by lncRNAs. Qian *et al.* (44) showed that the mammalian-imprinted *Dlk1-Gtl2* noncoding RNA inhibited PI3K-mTOR signaling, which in turn maintained mitochondrial biogenesis and metabolic activity in check and protected cells from excessive reactive oxygen species (ROS). Another lncRNA, *NEAT1,* is up-regulated in nonalcoholic fatty liver disease and has been shown to influence the activation of mTOR. Overexpression of *NEAT1* in cells increased the levels of p-mTOR and p-S6K, and inhibition of *NEAT1* down-regulated mTOR signaling (45).

Using metabolic profiling, we investigated whether the increase in mTORC1 activity affected cellular metabolism. Compared with WT cells, *Hoxb3os*-KO displayed higher OCR at baseline and in response to FCCP without changes in ECAR. These data suggest that the defects in *Hoxb3os* knockout cells primarily result from alterations in mitochondrial respiration and not from glycolysis. This finding contrasts with previous studies that showed lower mitochondrial respiration and higher glycolysis in PKD (46). The molecular mechanism underlying the *Hoxb3os*-dependent metabolic abnormality is not yet clear. Mitochondria play a critical role in normal development and disease through various processes including metabolism and generation of ROS (47). Increased oxidative phosphorylation has been observed in many cancers, including lymphoma (48) and leukemia (49). It is possible that the enhanced mitochondrial respiration in *Hoxb3os* knockout cells is pathogenic because of an increase in ROS. Alternatively, deficiency of *Hoxb3os* may promote survival and prevent apoptosis of mutant cells. Future studies are required to examine these possibilities.

Finally, re-expression of *Hoxb3os* in mutant cells restored p-mTOR as well as p-RS6 and p-S6K to normal levels and partially rescued the metabolic abnormality. The *Hoxb3os* re-expression results provide further evidence for *Hoxb3os* regulation of mTORC1 and mitochondrial respiration. Whether the regulation of mTOR signaling by *Hoxb3os* is because of direct association of *Hoxb3os* with mTOR complex or is indirect remains to be determined.

Collectively, our data suggest that *Hoxb3os* regulates mTORC1 signaling and mitochondrial respiration. Because mTOR signaling is known to be dysregulated in ADPKD, our results provide important proof of concept for future studies on re-expressing *Hoxb3os* as a therapeutic strategy in ADPKD.

Experimental procedures

Animals and human studies

Ksp/Cre (50), *Pkhd1*/Cre (51), *Pkd1*$^{f/f}$ (52), and *Pkd2*$^{f/f}$ (52) mice were used in this study. The genetic background of the mice was C57BL/6, and animals of both sexes were used. All experiments involving animals were performed under the auspices of the Institutional Animal Care and Research Advisory Committees at the University of Minnesota. Human tissue from normal and ADPKD kidneys was provided by the Biological Materials Procurement Network (Bionet) at the University of Minnesota. Kidneys were immediately sealed in sterile bags, immersed in ice, and delivered to the laboratory. The protocol for the use of surgically discarded kidney tissues complied with federal regulations for excess surgical specimens obtained at the University of Minnesota Medical Center-Fairview Campus. All studies were approved by the Institutional Review Board at the University of Minnesota and complied with the Declaration of Helsinki principles.

Quantitative real-time PCR

Total RNA was extracted from mouse inner medullary collecting duct (mIMCD3) cell line or mouse kidneys using RNeasy Mini Kit (Qiagen, Germantown, MD) according to the manufacturer's protocol. mIMCD3 cells were purchased from American Type Culture Collection (ATCC) and were genotyped upon receipt using short tandem repeat (STR) DNA profiling. cDNA was synthesized using the iScript cDNA Synthesis Kit (Bio-Rad), and quantitative real-time PCR was performed with the iTAG Universal SYBR Green Supermix (Bio-Rad). Reactions were performed on the CFX Connect Real-Time System (Bio-Rad). Gene expression levels were normalized to U6 small nuclear RNA or 18S rRNA. Primers for detecting *Hoxb3os* expression were agagctggaactagaaact (forward) and aacctagcttattactgcttc (reverse).

RNA-Seq

RNA extracted from mouse kidney was checked for quality and sequenced on Illumina instruments. Paired-end reads were checked for quality using FastQC (v0.11.2) and FastQ Screen (v0.4.4) and were quality trimmed using fastq-mcf (ea-utils, v1.1.2-806). Trimmed reads were aligned to the mouse reference genome (UCSC mm10 version from iGenomes) using STAR (v2.4.2a) and known transcripts from GENCODE (vM9). Cufflinks (v2.2.1) was then used for reference annotation–based transcript assembly (RABT) of the transcriptome for each of the individual samples. The individual assemblies were then merged and annotated using GENCODE (vM9) into a single collection of transcripts using Cuffmerge. Expression quantification and differential expression analysis were performed on the transcripts using RSEM (v1.2.22) and edgeR, respectively. Raw and processed data have been deposited in NCBI GEO under accession number GSE108864. For the GapmeR knockdown experiment, poly(A)$^+$ mRNA was used to create an Illumina TruSeq library that was sequenced (50 cycles paired-end) on an Illumina HiSeq 2500 System to a depth of greater than 30 million reads per sample. Reads were quality checked (FastQC v0.11.5), adapter trimmed (Trimmomatic v0.32), and

mapped to the GRCm38 reference genome with STAR (2.4.2a_modified). Mapped reads were indexed and sorted with SAMtools (v1.0). The number of reads mapping to each transcript in ENSEMBL annotation set (v84) was estimated with summarizeOverlaps (v1.8.3). Moderated $\log_2$-fold change values and Benjamini-Hochberg–corrected p values were calculated using DESeq2 (1.12.3). bigWig files were created using rtracklayer (1.32.2) and scaled based on the normalization in DESeq2.

lncRNA identification pipeline

Transcripts with log cpm >-1 and false discovery rate <0.05 were considered statistically significant and were included in the analysis. PhyloCSF was used to assess the protein-coding potential of *de novo* transcripts by examining the overrepresentation of evolutionary signatures characteristic of alignments of conserved coding regions such as the high frequencies of synonymous codon substitutions and conservative amino acid substitution. For each locus, the ORF with maximum PhyloCSF score was taken.

RNA fractionation

Freshly harvested adult mouse kidney was cut into small pieces, re-suspended in 800 μl cytoplasmic buffer (10 mM Tris-HCl, pH 7.4, 10 mM NaCl, 3 mM $MgCl_2$, 10% glycerol, 0.5% NP40, and 0.5 mM DTT). Samples were homogenized with a Dounce homogenizer into a single cell suspension and centrifuged at 13000 $\times$ g for 2 min to obtain the cytoplasmic fraction. The process was repeated twice, and the three fractions containing cytosolic RNA were combined. The remaining pellet contained nuclear RNA. RNA was extracted from cytosolic and nuclear fractions using the miRNeasy kit (Qiagen). Success of the fractionation procedure was confirmed by quantifying the levels of U6 small nuclear RNA and 18S RNA in each fraction.

In situ hybridization

Exiqon miRCURY LNA ISH FFPE Protocol (Exiqon miRCURY LNA ISH Optimization Kit 2, no. 90002) was utilized for *in situ* hybridization. Briefly, kidneys were perfused with 4% paraformaldehyde, fixed in paraformaldehyde for 48 h, transferred to 70% ethanol and embedded in paraffin blocks. Blocks were sectioned at 4 μm then incubated in an oven at 65 °C for 30 min before proceeding to deparaffinization. Sections were then washed with PBS three times then treated with proteinase K for 10 min at 37 °C. Double DIG-*Hoxb3os*–labeled detection probe (AGCAGAAGGTTGTGGTGGT) was hybridized to sections at 53 °C for 1 h. Anti–digoxigenin-AP Fab fragment antibody was used at 1:1000 dilution (Roche, 11093274910), and AP substrate was reapplied after 1 h. Slides were mounted with Eukitt mounting medium. Samples were examined using light microscopy.

Knockdown experiments

GapmeRs were purchased from Exiqon. mIMCD3 cells (2×10^5 cells/well) were seeded in a 6-well plate and grown for 24 h. After reaching 60–70% confluency, cells were transfected with 10 nM GapmeR against *Hoxb3os* (ATTACTGCTTCTTCCA) or negative control using Lipofectamine 3000. The cells were harvested 48 h after transfection and lysed in TRIzol (Invitrogen) for RNA extraction or in RIPA buffer (Sigma) for protein extraction.

CRISPR/Cas9 gene editing

Generation of the *Hoxb3os* mutant cell line was performed as described (53). Briefly, the following sgRNAs were used to generate three *Hoxb3os* mutant cell lines: sgRNA-1, caccgaaggtgattctgggagatct; sgRNA-2, caccgactgctcttaactaggccag. Each sgRNA was annealed and cloned into the pSpCas9(BB)-2A-puromycin construct (Addgene, no. 48139). Proper insertion of each sgRNA was confirmed by sequencing. One microgram of each sgRNA construct or empty vector was transfected into mIMCD3 cells using Lipofectamine 3000. Cells were trypsinized 72 h post transfection, and serial dilution was performed to obtain single-cell colonies in 96-well plates. *Hoxb3os* deleted clones were identified by PCR analysis of genomic DNA using the following detection primers: 5′-tgaggcgatcaatcttagcc-3′ (forward) and 5′-agctaaggtacacaacaccc-3′ (reverse).

RACE

RACE was performed using SMARTer® RACE 5′/3′ Kit from Clontech Laboratories, as described in the kit manual. The sequence of *Hoxb3os* primers used in RACE experiments were 5′-tcacgtgacagcctcattg-3′ (3′RACE) and 5′-aagagattccagcagatgca-3′ (5′RACE).

Western blotting

Cells were cultured in 6-well tissue culture plates. After reaching confluency, protein was extracted using RIPA lysis buffer (Sigma). Five micrograms of protein lysate was run on 4–12% Bis-tris or 2–8% Tris-acetate protein gels (Invitrogen) and transferred to nitrocellulose membranes using the wet transfer method. Blocking was performed using 5% milk in TBS with Tween for 1 h at room temperature. Membranes were incubated with antibodies at 1:1000 dilution in TBS with Tween with 5% BSA at 4 °C overnight. Secondary rabbit or mouse antibody was added at 1:20000 dilution in TBS with Tween for 1 h at room temperature. The following antibodies were purchased from Cell Signaling Technology: mTOR (2972), p-mTOR (2971), RS6 (2217), p-RS6 (2211), p-S6K (9234), 4E-BP1 (9451), p-4E–BP1 (9451). GAPDH was purchased from Santa Cruz (sc-25778) and used as loading control.

Extracellular flux measurements

Cells were seeded at 10,000 cells per well on Matrigel-coated Seahorse microplates for flux measurements on the XFe96 Extracellular Flux Analyzer (Agilent Seahorse Technologies). Glycolysis and oxidative phosphorylation were measured using the XF Cell Mito Stress Test Kit (Agilent). The stress tests require sequential addition of specific pathway inhibitors to query various aspects of these two metabolic pathways. The XF sensor cartridges were hydrated overnight at 37 °C without carbon dioxide in the Seahorse XF Calibrant Solution, as recommended in the manufacturer's protocol. The assay medium was Seahorse XF base medium (DMEM) supplemented with 5 mM pyruvate, 5 mM D-glucose, and 2 mM L-glutamine (pH 7.4). Oligomycin (1 mM), FCCP (1 mM), rotenone (0.5 mM), and antimy-

cin (0.5 mM) were added to the ports. Both ECAR and OCR measurements were performed at 8-min intervals (2 min mixing, 2 min recovery, and 4 min measuring) for 3 h using the Seahorse XFe96 analyzer. Measurements were recorded from three biological replicates with eight technical replicates per experiment. All data were normalized to cell number.

Statistical analysis

Student's two-tailed unpaired *t* test was used for pairwise comparisons. Analysis of variance (ANOVA) followed by Tukey's post hoc test were used for multiple comparisons. $p < 0.05$ was considered to be significant.

Author contributions—K. A. conceptualization; K. A., S. F., M. K., M. D. G., and C. X. formal analysis; K. A. and S. F. investigation; K. A., S. C. C., S. A., A. M., and D. L. methodology; K. A. writing-original draft; S. F. validation; M. K., M. D. G., and C. X. resources; M. K. and C. X. data curation; V. P., C. X., and P. I. supervision; P. I. funding acquisition.

Acknowledgments—We thank Jeremy Herrera for his help in performing ISH experiments. We also thank Stefan Somlo for providing the Pkd1$^{f/f}$ and Pkd2$^{f/f}$ mice. We thank Dr. Ameeta Kelekar and the MN Partnership Infrastructure Award MNP IF 16.09 for access to the Seahorse XFe96 Analyzer.

References

1. Grantham, J. J., Gardner, K. D., and PKR Foundation (1985) *Problems in Diagnosis and Management of Polycystic Kidney Disease: Proceedings of the First International Workshop on Polycystic Kidney Disease*. PKR Foundation, Kansas City, MO.
2. Iglesias, C. G., Torres, V. E., Offord, K. P., Holley, K. E., Beard, C. M., and Kurland, L. T. (1983) Epidemiology of adult polycystic kidney disease, Olmsted County, Minnesota: 1935–1980. *Am. J. Kidney. Dis.* **2,** 630–639 CrossRef Medline
3. Harris, P. C., and Torres, V. E. (2002) Polycystic kidney disease, autosomal dominant. In *GeneReviews*® (Adam, M. P., Ardinger, H. H., Pagon, R. A., Wallace, S. E., Bean, L. J. H., Mefford, H. C., Stephens, K., Amemiya, A., and Ledbetter, N., eds.), University of Washington, Seattle, WA.
4. Audrézet, M. P., Corbiere, C., Lebbah, S., Morinière, V., Broux, F., Louillet, F., Fischbach, M., Zaloszyc, A., Cloarec, S., Merieau, E., Baudouin, V., Deschênes, G., Roussey, G., Maestri, S., Visconti, C., et al. (2016) Comprehensive PKD1 and PKD2 mutation analysis in prenatal autosomal dominant polycystic kidney disease. *J. Am. Soc. Nephrol.* **27,** 722–729 CrossRef Medline
5. Cornec-Le Gall, E., Torres, V. E., and Harris, P. C. (2017) Genetic complexity of autosomal dominant polycystic kidney and liver diseases. *J. Am. Soc. Nephrol.* **29,** 13–23 CrossRef Medline
6. Hateboer, N., v Dijk, M. A., Bogdanova, N., Coto, E., Saggar-Malik, A. K., San Millan, J. L., Torra, R., Breuning, M., and Ravine, D. (1999) Comparison of phenotypes of polycystic kidney disease types 1 and 2. European PKD1-PKD2 Study Group. *Lancet* **353,** 103–107 CrossRef Medline
7. Hughes, J., Ward, C. J., Peral, B., Aspinwall, R., Clark, K., San Millán, J. L., Gamble, V., and Harris, P. C. (1995) The polycystic kidney disease 1 (PKD1) gene encodes a novel protein with multiple cell recognition domains. *Nat. Genet.* **10,** 151–160 CrossRef Medline
8. Kurbegovic, A., Kim, H., Xu, H., Yu, S., Cruanès, J., Maser, R. L., Boletta, A., Trudel, M., and Qian, F. (2014) Novel functional complexity of polycystin-1 by GPS cleavage *in vivo*: Role in polycystic kidney disease. *Mol. Cell Biol.* **34,** 3341–3353 CrossRef Medline
9. Mochizuki, T., Wu, G. Q., Hayashi, T., Xenophontos, S. L., Veldhuisen, B., Saris, J. J., Reynolds, D. M., Cai, Y. Q., Gabow, P. A., Pierides, A., Kimberling, W. J., Breuning, M. H., Deltas, C. C., Peters, D. J. M., and Somlo, S. (1996) PKD2, a gene for polycystic kidney disease that encodes an integral membrane protein. *Science* **272,** 1339–1342 CrossRef Medline
10. Qian, F., Germino, F. J., Cai, Y., Zhang, X., Somlo, S., and Germino, G. G. (1997) PKD1 interacts with PKD2 through a probable coiled-coil domain. *Nat. Genet.* **16,** 179–183 CrossRef Medline
11. González-Perrett, S., Kim, K., Ibarra, C., Damiano, A. E., Zotta, E., Batelli, M., Harris, P. C., Reisin, I. L., Arnaout, M. A., and Cantiello, H. F. (2001) Polycystin-2, the protein mutated in autosomal dominant polycystic kidney disease (ADPKD), is a Ca^{2+}-permeable nonselective cation channel. *Proc. Natl. Acad. Sci. U.S.A.* **98,** 1182–1187 CrossRef Medline
12. Aguiari, G., Banzi, M., Gessi, S., Cai, Y. Q., Zeggio, E., Manzati, E., Piva, R., Lambertini, E., Ferrari, L., Peters, D. J., Lanza, F., Harris, P. C., Borea, P. A., Somlo, S., and Del Senno, L. (2004) Deficiency of polycystin-2 reduces Ca^{2+} channel activity and cell proliferation in ADPKD lymphoblastoid cells. *FASEB J.* **18,** 884–886 CrossRef Medline
13. Hanaoka, K., and Guggino, W. B. (2000) cAMP regulates cell proliferation and cyst formation in autosomal polycystic kidney disease cells. *J. Am. Soc. Nephrol.* **11,** 1179–1187 Medline
14. Song, X., Di Giovanni, V., He, N., Wang, K., Ingram, A., Rosenblum, N. D., and Pei, Y. (2009) Systems biology of autosomal dominant polycystic kidney disease (ADPKD): Computational identification of gene expression pathways and integrated regulatory networks. *Hum. Mol. Genet.* **18,** 2328–2343 CrossRef Medline
15. Boca, M., Distefano, G., Qian, F., Bhunia, A. K., Germino, G. G., and Boletta, A. (2006) Polycystin-1 induces resistance to apoptosis through the phosphatidylinositol 3-kinase/Akt signaling pathway. *J. Am. Soc. Nephrol.* **17,** 637–647 CrossRef Medline
16. Lin, F., Hiesberger, T., Cordes, K., Sinclair, A. M., Goldstein, L. S., Somlo, S., and Igarashi, P. (2003) Kidney-specific inactivation of the KIF3A subunit of kinesin-II inhibits renal ciliogenesis and produces polycystic kidney disease. *Proc. Natl. Acad. Sci. U.S.A.* **100,** 5286–5291 CrossRef Medline
17. Baba, M., Furihata, M., Hong, S. B., Tessarollo, L., Haines, D. C., Southon, E., Patel, V., Igarashi, P., Alvord, W. G., Leighty, R., Yao, M., Bernardo, M., Ileva, L., Choyke, P., Warren, M. B., Zbar, B., Linehan, W. M., and Schmidt, L. S. (2008) Kidney-targeted Birt-Hogg-Dube gene inactivation in a mouse model: Erk1/2 and Akt-mTOR activation, cell hyperproliferation, and polycystic kidneys. *J. Natl. Cancer Inst.* **100,** 140–154 CrossRef Medline
18. Ma, L., Bajic, V. B., and Zhang, Z. (2013) On the classification of long non-coding RNAs. *RNA Biol.* **10,** 925–933 CrossRef Medline
19. Yang, G. D., Lu, X. Z., and Yuan, L. J. (2014) LncRNA: A link between RNA and cancer. *Biochim. Biophys. Acta* **1839,** 1097–1109 CrossRef Medline
20. Parasramka, M. A., Maji, S., Matsuda, A., Yan, I. K., and Patel, T. (2016) Long non-coding RNAs as novel targets for therapy in hepatocellular carcinoma. *Pharmacol. Ther.* **161,** 67–78 CrossRef Medline
21. Fatima, R., Akhade, V. S., Pal, D., and Rao, S. M. (2015) Long noncoding RNAs in development and cancer: Potential biomarkers and therapeutic targets. *Mol. Cell Ther.* **3,** 5 CrossRef Medline
22. Schmitt, A. M., and Chang, H. Y. (2016) Long noncoding RNAs in cancer pathways. *Cancer Cell* **29,** 452–463 CrossRef Medline
23. Wang, F., Ying, H. Q., He, B. S., Pan, Y. Q., Deng, Q. W., Sun, H. L., Chen, J., Liu, X., and Wang, S. K. (2015) Upregulated lncRNA-UCA1 contributes to progression of hepatocellular carcinoma through inhibition of miR-216b and activation of FGFR1/ERK signaling pathway. *Oncotarget* **6,** 7899–7917 CrossRef Medline
24. Hessels, D., and Schalken, J. A. (2009) The use of PCA3 in the diagnosis of prostate cancer. *Nat. Rev. Urol.* **6,** 255–261 CrossRef Medline
25. Ji, P., Diederichs, S., Wang, W., Böing, S., Metzger, R., Schneider, P. M., Tidow, N., Brandt, B., Buerger, H., Bulk, E., Thomas, M., Berdel, W. E., Serve, H., and Müller-Tidow, C. (2003) MALAT-1, a novel noncoding RNA, and thymosin β4 predict metastasis and survival in early-stage non-small cell lung cancer. *Oncogene* **22,** 8031–8041 CrossRef Medline
26. Ying, L., Chen, Q., Wang, Y. W., Zhou, Z. H., Huang, Y. R., and Qiu, F. (2012) Upregulated MALAT-1 contributes to bladder cancer cell migration by inducing epithelial-to-mesenchymal transition. *Mol. Biosyst.* **8,** 2289–2294 CrossRef Medline
27. Lin, R., Maeda, S., Liu, C., Karin, M., and Edgington, T. S. (2007) A large noncoding RNA is a marker for murine hepatocellular carcinomas and a

spectrum of human carcinomas. *Oncogene* **26,** 851–858 CrossRef Medline
28. Ji, Q., Zhang, L., Liu, X., Zhou, L., Wang, W., Han, Z., Sui, H., Tang, Y., Wang, Y., Liu, N., Ren, J., Hou, F., and Li, Q. (2014) Long non-coding RNA MALAT1 promotes tumour growth and metastasis in colorectal cancer through binding to SFPQ and releasing oncogene PTBP2 from SFPQ/PTBP2 complex. *Br. J. Cancer* **111,** 736–748 CrossRef Medline
29. Tano, K., Mizuno, R., Okada, T., Rakwal, R., Shibato, J., Masuo, Y., Ijiri, K., and Akimitsu, N. (2010) MALAT-1 enhances cell motility of lung adenocarcinoma cells by influencing the expression of motility-related genes. *FEBS Lett.* **584,** 4575–4580 CrossRef Medline
30. Long, J., Badal, S. S., Ye, Z., Wang, Y., Ayanga, B. A., Galvan, D. L., Green, N. H., Chang, B. H., Overbeek, P. A., and Danesh, F. R. (2016) Long noncoding RNA Tug1 regulates mitochondrial bioenergetics in diabetic nephropathy. *J. Clin. Invest.* **126,** 4205–4218 CrossRef Medline
31. Igarashi, P., and Somlo, S. (2007) Polycystic kidney disease. *J. Am. Soc. Nephrol.* **18,** 1371–1373 CrossRef Medline
32. Patel, V., Chowdhury, R., and Igarashi, P. (2009) Advances in the pathogenesis and treatment of polycystic kidney disease. *Curr. Opin. Nephrol. Hypertens.* **18,** 99–106 CrossRef Medline
33. Lin, M. F., Jungreis, I., and Kellis, M. (2011) PhyloCSF: A comparative genomics method to distinguish protein coding and non-coding regions. *Bioinformatics* **27,** i275–i282 CrossRef Medline
34. De Kumar, B., and Krumlauf, R. (2016) HOXs and lincRNAs: Two sides of the same coin. *Sci. Adv.* **2,** e1501402 CrossRef Medline
35. Hay, N., and Sonenberg, N. (2004) Upstream and downstream of mTOR. *Genes Dev.* **18,** 1926–1945 CrossRef Medline
36. Foster, K. G., and Fingar, D. C. (2010) Mammalian target of rapamycin (mTOR): Conducting the cellular signaling symphony. *J. Biol. Chem.* **285,** 14071–14077 CrossRef Medline
37. Sarbassov, D. D., Guertin, D. A., Ali, S. M., and Sabatini, D. M. (2005) Phosphorylation and regulation of Akt/PKB by the Rictor-mTOR complex. *Science* **307,** 1098–1101 CrossRef Medline
38. Schieke, S. M., Phillips, D., Mccoy, J. P., Jr., Aponte, A. M., Shen, R. F., Balaban, R. S., and Finkel, T. (2006) The mammalian target of rapamycin (mTOR) pathway regulates mitochondrial oxygen consumption and oxidative capacity. *J. Biol. Chem.* **281,** 27643–27652 CrossRef Medline
39. Emmrich, S., Streltsov, A., Schmidt, F., Thangapandi, V. R., Reinhardt, D., and Klusmann, J. H. (2014) LincRNAs MONC and MIR100HG act as oncogenes in acute megakaryoblastic leukemia. *Mol. Cancer* **13,** 171 CrossRef Medline
40. Li, L., Liu, B., Wapinski, O. L., Tsai, M. C., Qu, K., Zhang, J., Carlson, J. C., Lin, M., Fang, F., Gupta, R. A., Helms, J. A., and Chang, H. Y. (2013) Targeted disruption of *Hotair* leads to homeotic transformation and gene derepression. *Cell Rep.* **5,** 3–12 CrossRef Medline
41. Wang, K. C., Yang, Y. W., Liu, B., Sanyal, A., Corces-Zimmerman, R., Chen, Y., Lajoie, B. R., Protacio, A., Flynn, R. A., Gupta, R. A., Wysocka, J., Lei, M., Dekker, J., Helms, J. A., and Chang, H. Y. (2011) A long noncoding RNA maintains active chromatin to coordinate homeotic gene expression. *Nature* **472,** 120–124 CrossRef Medline
42. Warner, G., Hein, K. Z., Nin, V., Edwards, M., Chini, C. C. S., Hopp, K., Harris, P. C., Torres, V. E., and Chini, E. N. (2016) Food restriction ameliorates the development of polycystic kidney disease. *J. Am. Soc. Nephrol.* **27,** 1437–1447 CrossRef Medline
43. Braun, W. E., Schold, J. D., Stephany, B. R., Spirko, R. A., and Herts, B. R. (2014) Low-dose rapamycin (sirolimus) effects in autosomal dominant polycystic kidney disease: An open-label randomized controlled pilot study. *Clin. J. Am. Soc. Nephrol.* **9,** 881–888 CrossRef Medline
44. Qian, P. X., He, X. C., Paulson, A., Li, Z. R., Tao, F., Perry, J. M., Guo, F. L., Zhao, M., Zhi, L., Venkatraman, A., Haug, J. S., Parmely, T., Li, H., Dobrowsky, R. T., Ding, W. X., Kono, T., Ferguson-Smith, A. C., and Li, L. H. (2016) The *Dlk1-Gtl2* locus preserves LT-HSC function by inhibiting the PI3K-mTOR pathway to restrict mitochondrial metabolism. *Cell Stem Cell* **18,** 214–228 CrossRef Medline
45. Wang, X. (2017) Down-regulation of lncRNA-NEAT1 alleviated the nonalcoholic fatty liver disease via mTOR/S6K1 signaling pathway. *J. Cell Biochem.* **119,** 1567–1574
46. Rowe, I., Chiaravalli, M., Mannella, V., Ulisse, V., Quilici, G., Pema, M., Song, X. W. W., Xu, H. X., Mari, S., Qian, F., Pei, Y., Musco, G., and Boletta, A. (2013) Defective glucose metabolism in polycystic kidney disease identifies a new therapeutic strategy. *Nat. Med.* **19,** 488–493 CrossRef Medline
47. Pelicano, H., Xu, R. H., Du, M., Feng, L., Sasaki, R., Carew, J. S., Hu, Y. M., Ramdas, L., Hu, L. M., Keating, M. J., Zhang, W., Plunkett, W., and Huang, P. (2006) Mitochondrial respiration defects in cancer cells cause activation of Akt survival pathway through a redox-mediated mechanism. *J. Cell Biol.* **175,** 913–923 CrossRef Medline
48. Birkenmeier, K., Dröse, S., Wittig, I., Winkelmann, R., Käfer, V., Döring, C., Hartmann, S., Wenz, T., Reichert, A. S., Brandt, U., and Hansmann, M. L. (2016) Hodgkin and Reed-Sternberg cells of classical Hodgkin lymphoma are highly dependent on oxidative phosphorylation. *Int. J. Cancer* **138,** 2231–2246 CrossRef Medline
49. Kuntz, E. M., Baquero, P., Michie, A. M., Dunn, K., Tardito, S., Holyoake, T. L., Helgason, G. V., and Gottlieb, E. (2017) Targeting mitochondrial oxidative phosphorylation eradicates therapy-resistant chronic myeloid leukemia stem cells. *Nat. Med.* **23,** 1234–1240 CrossRef Medline
50. Shao, X. L., Somlo, S., and Igarashi, P. (2002) Epithelial-specific Cre/lox recombination in the developing kidney and genitourinary tract. *J. Am. Soc. Nephrol.* **13,** 1837–1846 CrossRef Medline
51. Patel, V., Li, L., Cobo-Stark, P., Shao, X. L., Somlo, S., Lin, F. M., and Igarashi, P. (2008) Acute kidney injury and aberrant planar cell polarity induce cyst formation in mice lacking renal cilia. *Hum. Mol. Genet.* **17,** 1578–1590 CrossRef Medline
52. Shibazaki, S., Yu, Z. H., Nishio, S., Tian, X., Thomson, R. B., Mitobe, M., Louvi, A., Velazquez, H., Ishibe, S., Cantley, L. G., Igarashi, P., and Somlo, S. (2008) Cyst formation and activation of the extracellular regulated kinase pathway after kidney specific inactivation of Pkd1. *Hum. Mol. Genet.* **17,** 1505–1516 CrossRef Medline
53. Ran, F. A., Hsu, P. D., Wright, J., Agarwala, V., Scott, D. A., and Zhang, F. (2013) Genome engineering using the CRISPR-Cas9 system. *Nat. Protoc.* **8,** 2281–2308 CrossRef Medline